Time-varying mobility and turnover of actomyosin ring components during cytokinesis in *Schizosaccharomyces pombe*

Anton Kamnev[a], Saravanan Palani[a,†,‡], Paola Zambon[a,†], Tom Cheffings[a], Nigel Burroughs[a,b], and Mohan K. Balasubramanian[a,*]

[a]Centre for Mechanochemical Cell Biology and Division of Biomedical Sciences, Warwick Medical School, and [b]Department of Mathematics, University of Warwick, Coventry CV4 7AL, UK

ABSTRACT **Cytokinesis in many eukaryotes is dependent on a contractile actomyosin ring (AMR), composed of F-actin, myosin II, and other actin and myosin II regulators. Through fluorescence recovery after photobleaching experiments, many components of the AMR have been shown to be mobile and to undergo constant exchange with the cytosolic pools. However, how the mobility of its components changes at distinct stages of mitosis and cytokinesis has not been addressed. Here, we describe the mobility of eight *Schizosaccharomyces pombe* AMR proteins at different stages of mitosis and cytokinesis using an approach we have developed. We identified three classes of proteins, which showed 1) high (Ain1, Myo2, Myo51), 2) low (Rng2, Mid1, Myp2, Cdc12), and 3) cell cycle–dependent (Cdc15) mobile fractions. We observed that the F-BAR protein Cdc15 undergoes a 20–30% reduction in its mobile fraction after spindle breakdown and initiation of AMR contraction. Moreover, our data indicate that this change in Cdc15 mobility is dependent on the septation initiation network (SIN). Our work offers a novel strategy for estimating cell cycle–dependent mobile protein fractions in cellular structures and provides a valuable dataset, that is of interest to researchers working on cytokinesis.**

Monitoring Editor
Thomas Pollard
Yale University

Received: Sept 15, 2020
Revised: Dec 1, 2020
Accepted: Dec 7, 2020

INTRODUCTION

Cell division in many eukaryotes requires formation of a functional actomyosin ring (AMR), comprising F-actin, tropomyosin, myosin motors, membrane scaffold proteins, actin cross-linkers, and other proteins (Schroeder, 1973; Fujiwara and Pollard, 1976; Nurse *et al.*, 1976; Chang *et al.*, 1996; Balasubramanian *et al.*, 1998; Wu and Pollard, 2005; Matsuyama *et al.*, 2006; Wood *et al.*, 2012; Pollard and O'Shaughnessy, 2019). Following anaphase, the AMR contracts with simultaneous deposition of a new membrane and the division septum (in yeast and fungi) leading to fission of a cell into two daughters. In many organisms, multiple components of the AMR undergo rapid turnover (Yumura, 2001; Guha *et al.*, 2005). Consistently, many components of the AMR in *Schizosaccharomyces pombe* undergo constant exchange with the cytosolic pool as well. These proteins include actin (Pelham and Chang, 2002; Chew *et al.*, 2017), myosin-II (Wong *et al.*, 2002; Clifford *et al.*, 2008; Laporte *et al.*, 2011; Okada *et al.*, 2019), anillin-like protein Mid1 (Clifford *et al.*, 2008; Zhang *et al.*, 2010) and F-BAR protein Cdc15 (Clifford *et al.*, 2008; Roberts-Galbraith *et al.*, 2009; Mcdonald *et al.*, 2015).

To date, most of the studies addressing protein turnover in the AMR have used the method of fluorescent recovery after photobleaching (FRAP). FRAP analysis normally relies on many assumptions—some of which have not been proven in *S. pombe*. In particular, FRAP experiments often assume that the proportion of bleached fluorophores is insignificant compared with the total amount of the fluorophore in the cell. However, for many AMR components, it has been shown that a significant fraction of the protein is localized to the AMR during cytokinesis (Wu and Pollard, 2005). This fraction can be as high as 50% of the total protein (Table 1), and is thus inconsistent with the assumption. In the present study, we address the question of whether the turnover of AMR components changes during different stages of mitosis and cytokinesis and provide a detailed temporal map of the mobile fractions relative to cell cycle progression.

This article was published online ahead of print in MBoC in Press (http://www.molbiolcell.org/cgi/doi/10.1091/mbc.E20-09-0588) on December 16, 2020.

†These authors contributed equally.

‡Present address: Department of Biochemistry, Indian Institute of Science, Bangalore 560012, India.

*Address correspondence to: Mohan K. Balasubramanian (M.K.Balasubramanian@warwick.ac.uk).

Abbreviations used: ROI, region of interest; SIN, septation initiation network.

TABLE 1: Changes in local accumulation and protein turnover during cytokinesis.

	Cell cycle stage		Published data		Current study		
Protein	Phase	Time after SPB separation	Protein % in AMRa	Fm, %	Raw Fm, %	Est Fm, %	FLIP, %
Ain1	Node assembly	–20 min	—	—	—	—	—
	Node coalescence	0 min	0	—	—	—	—
	Anaphase B	+10 min	10	—	55	97	42
	Contraction	+35 min	12	—	53	93	40
Cdc12	Node assembly	–20 min	—	70[b]	—	—	—
	Node coalescence	0 min	50	—	—	—	—
	Anaphase B	+10 min	18	80[c]	6	21	15
	Contraction	+35 min	50	—	9	30	21
Cdc15	Node assembly	–20 min	—	75[b]	—	—	—
	Node coalescence	0 min	3	—	—	—	—
	Anaphase B	+10 min	30	60 [d,e,f,g]	52	72	20
	Contraction	+35 min	40	—	28	47	19
Mid1	Node assembly	–20 min	—	68 [b,h]	—	—	—
	Node coalescence	0 min	—	20 [h]	—	—	—
	Anaphase B	+10 min	50	7 [d]	5	13	8
	Contraction	+35 min	—	—	5	20	15
Myo2	Node assembly	–20 min	—	60 [b]	—	—	—
	Node coalescence	0 min	45	—	—	—	—
	Anaphase B	+10 min	40	65 [d]	46	75	29
	Contraction	+35 min	37	38 [i, j]	51	86	35
Myo51	Node assembly	–20 min	—	—	—	—	—
	Node coalescence	0 min	—	—	—	—	—
	Anaphase B	+10 min	—	—	53	82	29
	Contraction	+35 min	—	—	58	90	32
Myp2	Node assembly	–20 min	—	—	—	—	—
	Node coalescence	0 min	—	—	—	—	—
	Anaphase B	+10 min	20	—	—	—	—
	Contraction	+35 min	35	59 [i]	0	0	–11
Rng2	Node assembly	–20 min	—	75 [b]	—	—	—
	Node coalescence	0 min	—	—	—	—	—
	Anaphase B	+10 min	45	40 [d]	12	34	22
	Contraction	+35 min	—	—	12	31	19

Notes: Published data on mobile fraction (F_m) and relative amount in the AMR (percentage of cell total; Wu and Pollard, 2005) stratified into four time intervals by phase of cytokinesis and time since SPB separation (Wu *et al.*, 2003). Publications with unclear stage of cytokinesis for FRAP measurement were excluded from the analysis. Following data from current study are shown (average value for the time-interval): raw observed mobile fraction in AMR (Raw F_m), estimated true mobile fraction in AMR (Est F_m), and detected loss of intensity on unbleached side of the AMR (FLIP).
[a]Wu & Pollard, 2005; [b]Laporte *et al.*, 2011; [c]Yonetani *et al.*, 2008; [d]Clifford *et al.*, 2008; [e]Roberts-Galbraith *et al.*, 2009; [f]Roberts-Galbraith *et al.*, 2010; [g]Ullal *et al.*, 2016; [h]Zhang *et al.*, 2010; [i]Okada *et al.*, 2019; [j]Wollrab *et al.*, 2016.

RESULTS AND DISCUSSION

A method for determining cell cycle–dependent changes in mobile protein fractions during actomyosin ring formation and contraction

To evaluate the stage of mitosis or cytokinesis of a given cell, we used the length of the mitotic spindle and the diameter of the AMR as quantifiable proxies. In cells expressing *mCherry-atb2* and *mEGFP-myo2*, we found that the increase of spindle length during anaphase B and the decrease of AMR diameter during AMR contraction following spindle breakdown were linear (Figure 1A and Supplemental Figure 1A), in line with previous reports (Pelham and Chang, 2002). Because most *S. pombe* cells have roughly the same diameter of 3.7 ± 0.2 µm (Supplemental Figure 1B), we assumed that all AMRs had the same diameter at the onset of contraction. For simplicity, we defined a relative timeline for the processes of mitosis and cytokinesis (Figure 1B) where "-1" represents spindle pole body (SPB) separation

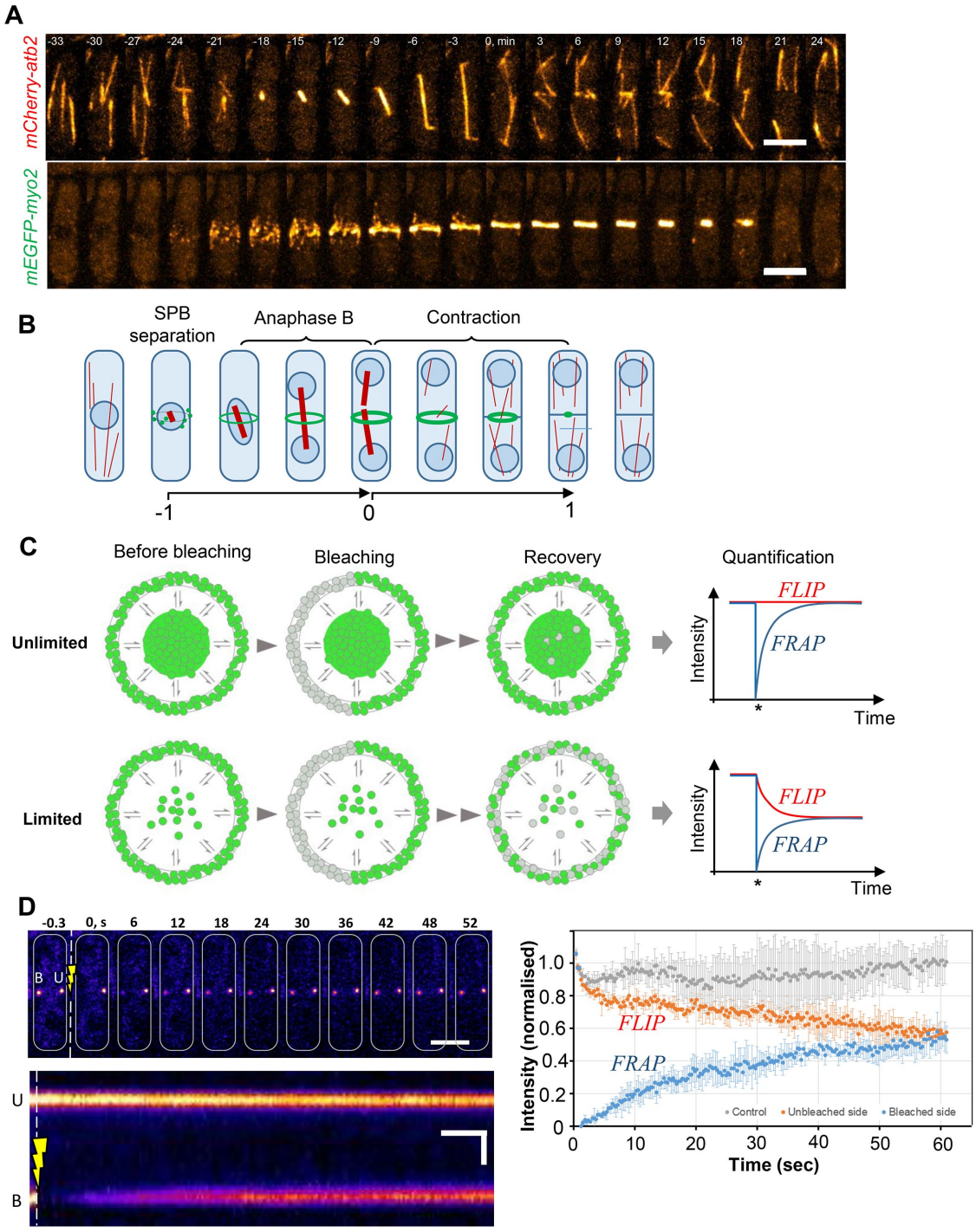

FIGURE 1: (A) AMR (*mEGFP-myo2*) and tubulin cytoskeleton (*mCherry-atb2*) in dividing *S. pombe* cell (scale bar = 5 µm). (B) *S. pombe* cell-cycle following changes in AMR microtubule cytoskeleton. (C) Protein exchange between bleached and unbleached domains of AMR after bleaching and resulting quantification. (D) Time-lapse series (scale bar = 5 µm), kymograph (scale bar = 1 µm vertical and 6 s horizontal) and quantification ($N = 4$; mean ± SD) of *mEGFP-myo2* in bleached (B, FRAP) and unbleached (U, FLIP) regions of the AMR.

and mitotic spindle assembly; "0" denotes spindle breakdown and the onset of cytokinesis; and "+1" represents the completion of AMR contraction (see the *Supplemental Methods* for details).

A key assumption in FRAP experiments is that the proportion of bleached protein is insignificant compared with its total amount available. However, the effect of a limited recovery pool is rarely taken in the account. The example below (Figure 1C), illustrates a how limited cytosolic pool affects observed recovery of an AMR protein with a mobile fraction of 100%. When the cytosolic pool of unbleached molecules is sufficiently large (Figure 1C, upper panel), the observed plateau of fluorescent recovery is equal to the mobile fraction of the protein (100%). However, when the amount of unbleached protein is limited, an exchange of molecules between bleached and unbleached domains of the AMR starts to dominate

the recovery (Figure 1C, bottom panel). This exchange results in partial recovery of the bleached domain, accompanied by loss of fluorescence in the unbleached domain. If half of the AMR is bleached, this will lead to significant differences between the observed plateau of fluorescent recovery (50%) and its true mobile fraction (100%).

To this end, we built a mathematical model to describe protein exchange between the cytosol and the AMR, allowing for finite amounts of protein in the system (see the *Supplemental Methods* for details). Specifically, our mathematical model showed that the true mobile fraction F_m could be estimated as

$$F_m = F'_m + F_{loss} \quad (1)$$

where F'_m is the FRAP value (protein recovery at the bleached side of AMR) and F_{loss} is the fluorescence loss after photobleaching (FLIP) at the unbleached side of AMR. Importantly, Formula 1 shows that estimation of the true mobile fraction does not require measurements of the concentration/amount of protein in the cytoplasm or AMR. This makes this approach generally applicable to a wide range of proteins, whose concentrations in the different compartments of *S. pombe* may not be known.

Finally, to demonstrate the implications of a limited cytosolic recovery pool and the importance of our correction to the FRAP-based measurement of protein mobility in living cells, we performed FRAP analysis of Myo2 mobility in the AMR. Myo2 is known to be highly mobile (Yumura, 2001; Wong *et al.*, 2002; Clifford *et al.*, 2008; Laporte *et al.*, 2011; Okada *et al.*, 2019) and ~40% of the cellular Myo2 was reported to localize to the AMR (Wu and Pollard, 2005; Table 1). Using cells expressing *mCherry-atb2* and *mEGFP-myo2*, we bleached a significant portion of the AMR (~30–50%; Supplemental Figure 1C) in cells at the onset of AMR contraction (spindle breakdown). The subsequent FRAP analysis of Myo-2 turnover showed a 50% recovery of its original value (Figure 1D, right panel); assuming an unlimited cytosolic pool, this gives the impression of a mobile fraction of 50%. However, the fluorescence intensity in the unbleached portion of the AMR displayed an exponential decrease immediately after photobleaching, showing a 40% loss of intensity from the original value. A loss of fluorescence of such magnitude cannot be explained by imaging-induced photobleaching alone and thus demonstrated that recovery in the bleached portion of the AMR is limited. Using Formula 1, we estimated the true mobility of the Myo2 protein as 90%.

Mapping changes in protein mobility during formation and contraction of the actomyosin ring

To quantify the mobility of AMR components as a function of AMR age, we generated fission yeast strains expressing *mCherry-atb2* for visualization of the mitotic spindle, and one of eight AMR proteins fused to either mEGFP or mNeonGreen. The following AMR components were chosen: the motor proteins Myo2 (Kitayama *et al.*, 1997; May *et al.*, 1997; Balasubramanian *et al.*, 1998), Myp2 (Bezanilla *et al.*, 1997; Motegi *et al.*, 1997), and Myo51 (Win *et al.*, 2001), the actin crosslinker Ain1 (Wu *et al.*, 2001), the F-BAR protein Cdc15 (Fankhauser *et al.*, 1995), formin Cdc12 (Chang *et al.*, 1997), the IQGAP-related protein Rng2 (Eng *et al.*, 1998), and the anillin-related protein Mid1 (Sohrmann *et al.*, 1996). In each strain, we performed FRAP-based measurements of the protein turnover at the AMR by bleaching a portion of the AMR in cells at different stages of mitosis and cytokinesis. For each cell, we recorded the length of the mitotic spindle or the diameter of the AMR, which were, in turn, used to calculated the age of the AMR. Finally, we used FRAP and FLIP data to estimate the true mobile fraction of the protein at the AMR of a given cell using Formula 1.

The results from these experiments allowed us to form (Figure 2, A–C, Supplemental Figure 2A, and Table 1) three categories of proteins based on their turnover in the AMR: 1) highly mobile proteins (Ain1, Myo51, and Myo2); 2) immobile or predominantly immobile proteins (Rng2, Mid1, Myp2, and Cdc12); and 3) proteins that displayed a dramatic change in their mobility (Cdc15). Consistent with our previous observation for Myo2 (Figure 1D), we observed that most of the AMR components used in this study displayed a loss of fluorescence intensity in the unbleached region of the AMR that could not be explained by imaging-induced loss of signal alone (only accounted for loss of 5–10%, Supplemental Figure 2B). Our results are in line with previous observations showing that the AMR contains a significant amount of the total protein in the cell for each of the selected AMR components (Figure 2C; Table 1). This effect was most prominent in highly mobile proteins where the loss from the unbleached region of the AMR was nearly 50% of the prebleach intensity (~40%, 30–35%, and 30–34% for Ain1, Myo2, and Myo51, respectively), resulting in a nearly twofold difference between raw and estimated true mobile fractions.

In thecase of Myp2, the intensity at the unbleached side of the AMR increased after bleaching (Figure 2A; Table 1), indicating ongoing recruitment of Myp2 to the AMR site. This observation was further supported by an independent measurement of Myp2 density per unit length of the AMR, showing a linear increase in the Myp2 density in the AMR during its contraction (Supplemental Figure 3A). Interestingly, our results contradicted a previous report on Myp2 turnover at the division site (Table 1, 56% recovery in contracting AMR; Okada *et al.*, 2019). In this publication, the measurement of the Myp2 mobile fraction was not adjusted to account for a constant delivery of the protein to the division site, which may have led to an overestimation of Myp2 mobility.

Finally, we compared mobile fractions of the chosen proteins before and after initiation of the AMR contraction. We selected two subsets from the final dataset: AMRs of age –0.8 to –0.2 (anaphase B) and AMRs of age 0 to +0.6 (contraction). Next, we explored whether there were statistically significant differences between the mean values of mobile fractions between those groups, using the Mann–Whitney U-test. After adjusting the p values for multiple hypothesis testing, we found that most of the studied proteins did not undergo significant changes in their mobile fraction between formation (anaphase B) and contraction of the AMR (Ain1, Cdc12, Mid1, Myo51, Rng2). Myo2 displayed an 11% increase in its mobility following initiation of AMR contraction ($p < 0.01$), while Cdc15 showed a dramatic 25% decrease in its mobility ($p < 0.001$). Interestingly, for all observed proteins, we found similar levels of FLIP through cell cycle progression (Figure 2C; Table 1), indicating that a significant proportion of the total protein amount remains in the AMR through its maturation and contraction phases for all observed AMR components.

Recent studies have highlighted the ability of AMR components such as Myo2 (Laplante *et al.*, 2016; Wollrab *et al.*, 2016), Cdc15, Cdc12, and Rng2 (Laplante *et al.*, 2016) to move along the AMR in the form of clusters. Such intra-AMR movement of proteins would affect the results of FRAP-based measurements of protein turnover. To address this issue, we followed the recovery of the protein after bleaching along the AMR using 3D imaging (Supplemental Figure 3B). With the exception of Cdc12, we could observe that most of the proteins in the study did not display signs of protein movement along the AMR (such as clusters or an intensity wave), indicating that the observed recovery of fluorescent intensity is mostly due to

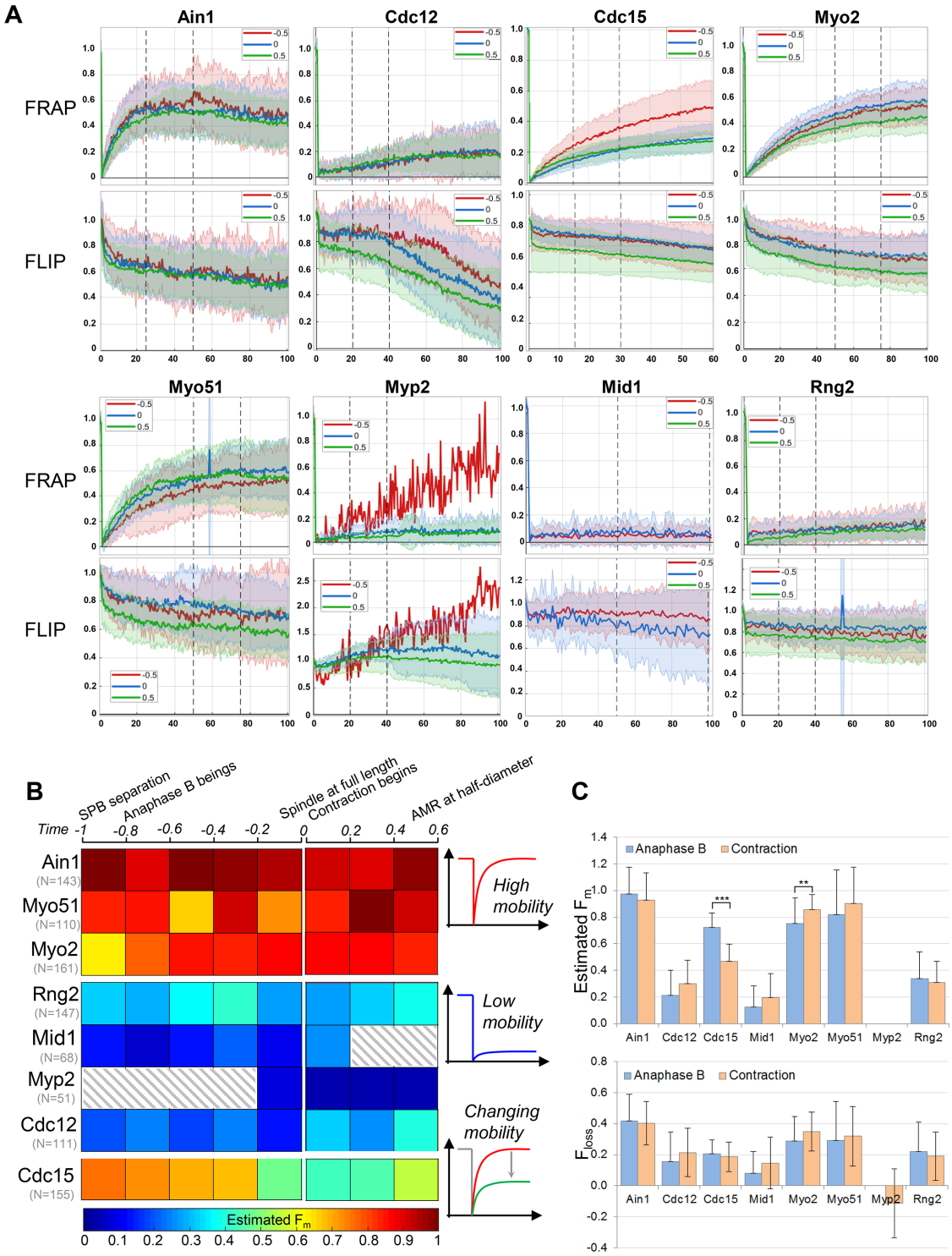

FIGURE 2: (A) FRAP and FLIP (mean ± SD) in AMR at early anaphase B (t = -0.5), onset of AMR contraction (t = 0), and contracting AMR (t = 0.5). Plateau for calculation of FLIP or FRAP values indicated by dotted lines. (B) Heat map of protein turnover (mean per time-interval). Age of the AMR and cytokinesis phases are shown at the top of the chart. Striped squares indicate time intevals with no detectable target protein or insufficient sample size ($N \leq 4$). (C) True mobile fraction (F_m) and FLIP at Anaphase B versus AMR contraction. Asterisks indicate statistically significant differences.

exchange of the protein through the cytoplasm. Interestingly, Cdc12 displayed movement of clusters from the unbleached domain. This could explain why a previous report on the Cdc12 mobile fraction in the AMR (Yonetani *et al.*, 2008; 80%, Table 1) differs from our estimate (21–30%). We hypthesize that the earlier study might have been affected by Cdc12 intra-AMR mobility, resulting in overestimation of the mobile fraction (the observed recovery would be the sum of two processes: Cdc12 mobility within the AMR and exchange

with cytoplasm). Our finding of limited exchange of Cdc12 between the AMR and cytoplasm indicates that during AMR contraction, Cdc12 might function as part of a larger molecular assembly, possible in the form of nanoscale nodes, similar in its composition to early AMR nodes (Laplante *et al.*, 2016).

Immobilization of Cdc15 in the actomyosin ring is induced by the septation initiation network pathway in late anaphase, and might be crucial for efficient cytokinesis

Our initial mobility screen revealed a biphasic mobility profile of the F-BAR protein Cdc15 (Figure 2 and Table 1), with a highly mobile phase during AMR formation (Fm ~70%) followed by a low-mobility phase starting at the onset of AMR contraction (Fm ~45%). These results were particularly fascinating because immobilization of Cdc15 has been suggested by previous in vitro and superresolution studies (Roberts-Galbraith *et al.*, 2010; Mcdonald *et al.*, 2017) and FRAP-based in vivo studies (Mcdonald *et al.*, 2015), supporting the proposed role of Cdc15 as a crucial protein scaffold and anchor for the contractile AMR. However, detailed monitoring of the changes in Cdc15 mobility during the lifespan of the AMR has not been performed yet. Therefore, it was of interest to compare the profile of Cdc15 mobility produced by our screen with existing models of Cdc15 action in cytokinesis.

Cdc15 is a crucial structural scaffold protein and is known to be cell cycle regulated (Fankhauser *et al.*, 1995; Swaffer *et al.*, 2018). It was previously indicated that Cdc15 localization and function during the early stages of AMR assembly might be regulated through de-/phosphorylation of its unstructured region and SH3 domain by the septation initiation network (SIN) and Pom1, respectively (Figure 3A; (Fankhauser *et al.*, 1995; Wachtler *et al.*, 2006; Roberts-Galbraith *et al.*, 2010; Mcdonald *et al.*, 2015; Bhattacharjee *et al.*, 2020). However, the exact function of the posttranslational modification dependent regulation of Cdc15 structure during cytokinesis is not fully understood yet.

To investigate whether the decrease in Cdc15 mobility at the onset of AMR contraction and efficient cytokinesis are related, we tracked Cdc15 mobility in cells with perturbed cytokinesis. Two components of the SIN signalling pathway were chosen: upstream GTPase Spg1 (Figure 3B; Schmidt *et al.*, 1997; Simanis, 2015) and downstream phosphatase Clp1, which is known to dephosphorylate Cdc15 during AMR assembly (Clifford *et al.*, 2008). Additionally, we included the truncated version of Cdc15 lacking its SH3 domain in our experiment (Roberts-Galbraith *et al.*, 2009). The Cdc15 SH3 domain is known to recruit proline-rich (PxxP) motif–containing proteins (such as Pxl1 and Fic1) to the AMR (Roberts-Galbraith *et al.*, 2009; Ren *et al.*, 2015; Bhattacharjee *et al.*, 2020) and thus is expected to play an important role in the formation of the AMR.

Our results showed an increase in Cdc15 mobility during both maturation and contraction of the AMR in the Δ*clp1* and *cdc15ΔSH3* backgrounds compared with wild-type (*wt* cells (Figure 3C). Interestingly, we could still detect a significant decrease in the Cdc15 mobile fraction following spindle breakdown in these strains, although the magnitude of this decrease was reduced when compared with *wt* cells (21–26% vs. 31%). Together with the fact that both Δ*clp1* and *cdc15ΔSH3* (unpublished data) backgrounds are able to generate functional AMR and properly initiate and complete cytokinesis (Supplementary Figure 4, A–C) while retaining high sensitivity to further perturbation of cytokinesis (Mishra *et al.*, 2004; Roberts-Galbraith *et al.*, 2009), these results indicate that Cdc15 immobilization in these cells is perturbed, but not significantly enough to cause cytokinesis failure.

Finally, we investigated the mobility of Cdc15 in the AMR of *spg1-106* cells, which are able to form an AMR but fail to initiate cytokinesis at restrictive temperature (Schmidt *et al.*, 1997; Balasubramanian *et al.*, 1998). First, we confirmed the phenotype of *spg1-106* cells at the restrictive temperature of 30°C and found that 50% of mitotic cells were unable to maintain an AMR at the division site, while the rest of the cells initiated contraction immediately followed by rupture of cells wall (Supplemental Figure 4, D–G). Measurement of Cdc15 turnover in the AMR in these cells at the restrictive temperature across the lifespan of the AMR revealed a lack of Cdc15 immobilization before and after spindle breakdown (Figure 3D).

Taken together, our measurements of the change in Cdc15 mobility during cytokinesis in Δ*clp1, cdc15ΔSH3* and *spg1-106* cells indicated that immobilization of Cdc15 in the AMR might be crucial for successful AMR contraction and cytokinesis. Together with its proposed role in AMR anchoring at the division site (McDonald *et al.*, 2015, 2017) we hypothesize that the observed positive correlation of Cdc15 immobilization and the efficiency of resulting cytokinesis might directly stem from the ability of Cdc15 to stabilize contractile AMR at the division site (Figure 3E). Here, activation of Cdc15 binding to both the plasma membrane and the AMR at the onset of AMR contraction leads to assembly of a Cdc15–dependent AMR–plasma membrane bridge, locking Cdc15 at the division site and stabilizing contractile AMR (detected as a drop in the Cdc15 mobile fraction in the AMR). In *wt* cells, this leads to successful septum deposition and cytokinesis. Partial or complete lack of Cdc15 activation before AMR contraction (in Δ*clp1* and *spg1-106* cells) leads to compromised anchoring and instability of the AMR at the division site. When anchoring is weakend but able to conduct contractile force from AMR under favorable conditions (Δ*clp1* cells), cytokinesis occurs but shows sensitivity to further perturbations. However, when proper assembly of the Cdc15 bridge fails completely (*spg1-106* cells), destabilization of the AMR results in failure of cytokinesis. It is unclear if Cdc15 immobilization at the AMR is indispensible for the AMR contraction or stability. Further studies with a focus on the activity of Cdc15 at the division site at the onset of AMR contraction would be required to identify the exact role of Cdc15 in the maintainance of the functional division site.

In summary, we have established a new, optimized FRAP-based protocol allowing measurements of protein mobility in the AMR of *S. pombe* across the lifespan of the AMR. We have demonstrated that most of the AMR components studied in this work presented limited cytoplasmic recovery pools, leading to underestimation of their mobile fraction as measured by unadjusted FRAP. Taken together, our results indicate that FRAP-based analysis of protein turnover in AMR is strongly affected by the capacity of the cytosolic recovery pool and thus needs to be properly corrected. Our FLIP-based method of correction for a limited cytosolic recovery pool allows such adjustment and therefore adds a new important tool for studies of cytokinesis. The dataset we provide should act as a starting point for further studies of protein mobility during cytokinesis in fission yeast.

In addition, our results provide the first clear evidence of Cdc15 immobilization in the AMR during late anaphase. We were able to show a biphasic profile of Cdc15 mobility consisting of a high-mobility phase during AMR formation and a low-mobility phase during its contraction. Moreover, the high temporal resolution of our method revealed that the immobilization of Cdc15 in late anaphase is an abrupt process, with Cdc15 reaching its minimum shortly before spindle breakdown and the initiation of

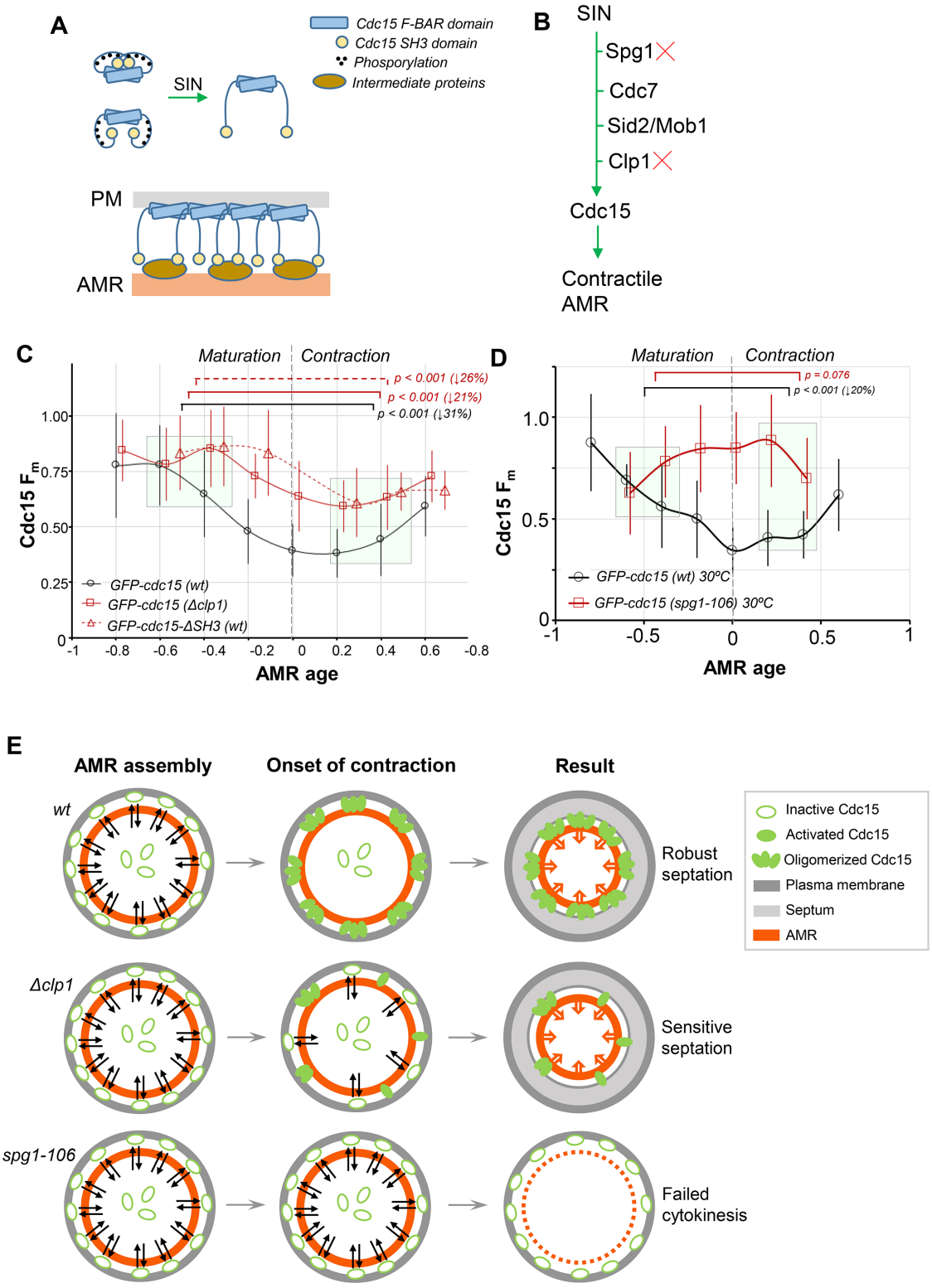

FIGURE 3: (A). SIN mediated Cdc15 activation & oligomerization at the plasma membrane (adopted from [Roberts-Galbraith *et al.*, 2010]). (B) Activation of Cdc15 by SIN pathway. (C) Changes in AMR mobility (mean ± SD) of Cdc15 in *wt*, Δ*clp1*, and *cdc15-ΔSH3* cells during cytokinesis. (D) AMR mobility (mean ± SD) of Cdc15 in *wt* versus *spg1-106* cells at restrictive temperature (30°C). (E) Model of Cdc15-dependent anchoring of AMR at the division site at the onset of AMR contraction.

AMR contraction. Finally, genetic manipulation of the SIN signalling pathway suggested a correlation between the drop in Cdc15 mobility at the end of the anaphase and the successful completion of cytokinesis. This finding provides a new angle to study the mechanisms of cytokinesis and provides new tools to probe Cdc15 function in vivo.

MATERIALS AND METHODS

Yeast genetics and culture methods

Log phase cells were grown and cultured in yeast extract medium with supplements (YES) at permissive temperature (24°C), as described earlier (Moreno *et al.*, 1991).

Paraformaldehyde fixation, DAPI, anillin blue, actin–phalloidin staining, and fluorescence microscopy

Asynchronous mid–log phase cells were grown at 24 or 30°C in YES and shifted to 36°C (*spg1-106*) for 3–4 h before fixation. For visualization of DAPI and anillin blue staining, cells were fixed with 4% paraformaldehyde and permeabilized for 10 min with 1% Triton X-100 at room temperature. Cells were washed three times with 1X PBS without Triton X-100 and stained with DAPI to visualize DNA and anillin blue to visualize septa. Still images were acquired using a spinning-disk confocal microscope (Andor Revolution XD imaging system; specifications are described in *Sample Preparation and Live Cell Imaging*).

Sample preparation and live cell imaging

For time-lapse live cell imaging, log-phase cells were grown at 24°C, concentrated from early log-phase culture, and spotted on a glass slide containing a YES agarose pad. Time-lapse movies were acquired in a 24°C incubation chamber for 1–2 h. Each sample was pre-incubated for 40–60 min prior to imaging in the incubation chamber. Time-lapse series were acquired using aspinning-disk confocal microscope (Andor TuCam imaging system, equipped with a 100× oil immersion 1.45NA Nikon Plan Apo lambda and 40× 1.3NA Nikon CFI Plan Fluor oil immersion objective lenses, confocal unit Yokogawa CSU-X1, Andor iXon Ultra EMCCD, and Andor iQ software). Images were acquired at resolution of either 69 (100× objective lens) or 162 nm/pxl (40× objective lens). Nine *z* slices of thickness 0.7 µm were taken for GFP and mCherry channels at every 3-min interval. Two laser lines of wavelength 488 and 561 nm were used for excitation. The imaging software Fiji was used to process the images.

Fluorescent recovery after photobleaching experiments

For analysis of protein turnover, cells were prepared as described in *Sample Preparation and Live Cell Imaging*. Cells were imaged using a spinning-disk confocal microscope (Andor TuCam imaging system, equipped with a 100× oil immersion 1.45NA Nikon Plan Apo lambda, confocal unit Yokogawa CSU-X1, Andor iXon Ultra EMCCD, FRAPPA Andor bleaching unit, and Andor iQ software). Images were acquired at a resolution of 69 nm/pixel. The fluorophores were photobleached using a 455-nm laser line. For each cell line, the minimum intensity and duration of the bleaching pulse were determined in order to minimize photobleaching of the cytosolic pool of target protein. The bleaching region of interest (ROI) was constructed as a 1 µm–wide line crossing one side of the AMR parallel to the longitudinal axis of the cell, generating an approximate 1 × 0.5–µm bleaching ROI that bleaches 30–50% of the AMR, depending on the AMR diameter. We chose a line ROI for bleaching primarily because of the speed of bleaching. Two laser lines of wavelength 488 and 561 nm were used for excitation. For measurement of the mobile fraction, all images were recorded as the 1-*Z* plane in the middle of the cell. For analysis of protein movement along the AMR, a *Z*-stack with intraslice spacing 0.3 µm was used (18 slices in total covering a *Z* range of 5.4 µm). First, the baseline of the protein signal in the AMR was recorded by three consecutive images taken as fast as possible (0.3 s on average for mobility measurement and 2–5 s for FRAP measurements of *Z*-stacks). Next, part of the AMR was bleached over 50–200 ms depending on the number of bleaching ROIs per field of view (five on the average). Finally, the FRAP signal was recorded as a sequence of 150 images taken at intervals of 0.3–1 s for mobility measurement and 2–5 s for FRAP measurements of *Z*-stacks (depending on fluorophore intensity and recovery half-life) for a total duration of 2–3 min. The time window of 2–3 min was chosen to maximize recovery of the proteins after bleaching (recovery half-life is on the order of seconds) and to minimize the impact of AMR contraction. To measure the impact of imaging-induced photobleaching, first some of the fields-of-view were selected to serve as control. We next conducted a FRAP experiment with one change: three to five FRAP ROIs were drawn at least 2 µm away from any cell containing AMR. FRAP ROIs were introduced to measure effect of FRAP-induced bleaching on neighburing cells in addition to imaging-induced photobleaching. This procedure was repeated until 20–30 cells with AMR were recorded. Finally, all images were saved as 16-bit .tiff raw data files.

The recorded data were then quantified using custom-written scripts in Fiji and Matlab. First, camera noise in the raw images was suppressed by applying a 2 × 2–pixel average filter (Fiji → Process → Filters → Mean). The mean intensity of the AMR was calculated in each image using a circular ROI 1 µm in diameter centered on either a bleached or unbleached cross-section of the AMR. In imaging-induced bleaching control recordings, both sides of the AMR were measured. A circular ROI was chosen to ensure measurement of intensity even when AMR had shifted in the image during acquisition (we observed minor submicrometer changes in the position of AMR, most probably due to AMR contraction). For each image, the mean intensity of the signal in the selected ROIs was then recorded and saved as an annotated CSV file. Finally, using a custom-written Matlab script and measurements from FRAP experiments, model parameters (such as mobile fraction) were extracted for each recording.

Spindle length information was collected for each cell in the FRAP analysis as 13 *z* slices of thickness 0.5 µm taken for the mCherry channel immediately before each FRAP sequence. The length of the spindle and the AMR diameter were measured in Fiji. Both the spindle length and the diameter of the AMRs were measured as the lengths of straight lines connecting ends of spindles or opposite sides of the AMR in the image. The measured data in CSV format were loaded into custom-written Matlab scripts.

Kymographs

Kymographs of changes of the fluorescent intensity in the AMR were built from the raw time-lapse images from FRAP experiments. First, camera noise in the image was suppressed by applying a 1 × 1–pixel average filter (Fiji → Process → Filters → Mean). The next kymograph was built along the line ROI of length ~5 µm and width 1 µm connecting opposite sides of the AMR using the ImageJ plugin KymoResliceWide (https://imagej.net/KymoResliceWide) as maximum-intensity projection along the width of the line ROI.

Image processing

Images were analyzed using Fiji. For live-cell imaging experiments, camera noise in the resulting stacks was suppressed by applying a 1 × 1–pixel average filter (Fiji → Process → Filters → Mean). Resulting images were projected along the *Z*-axis using maximum-intensity projection (Fiji → Image → Stacks → Z Project). ZY-projections were done from *Z*-stacks using the Fiji plugin 3D Project (Fiji → Image → Stacks → 3D Project).

Measurement of protein mobile fraction

First, we normalized data for FRAP and FLIP ROIs using acustom Matlab script (offset to background and normalization to the

average of the first three time-points. The next time-profile of intensity change was corrected for imaging-induced photobleaching using data from control cells. The resulting data were used to measure the mobile fraction (FRAP), and protein loss (FLIP) was extracted for each cell as average intensity in the last 40–100 frames (determined for each protein individueally depending on recovery kinetics). Finally the corrected mobile fraction was calculated using Formula 1. See the Supplemental Methods for full details.

Measurement of cell diameter variability

The diameter of each cell was measured from the *Z*-stack of DIC images, determined as the *Z*-slice that gave the largest measured value of the diameter.

Quantification of changes in Myp2-mApple density during cytokinesis

To measure the amount of Myp2 in *wt* AMRs, we took single-timepoint *Z*-stack images of *wt* cells expressing Myp2-mApple, using the DIC and GFP channels to capture ~50 cells containing AMRs at various stages of contraction. The difference between the cell diameter (measured from DIC) and AMR diameter (measured from the Myp2 signal) was used as a measure of how much the AMR had already contracted. AMR fluorescence intensity was measured from summed intensity projections. The Myp2 signal was used to draw a polygon ROI around the AMR, and the average Myp2 intensity in this region was measured. We subtracted the background Myp2 signal (measured from other regions of the cell) and then multiplied this value by the area of the AMR ROI to obtain the total fluorescence intensity of Myp2 in the AMR. To calculate the intensity/length, we then divided these values by the AMR circumference.

Statistical analysis

In Figures 2B and 3, C and D, *p* values were obtained by a Mann–Whitney U-test. All *p* values were adjusted for multiple hypothesis testing using Bonferroni correction. Statistical analysis was performed using a MATLAB software package.

ACKNOWLEDGMENTS

We thank Darius Koester, Tomoyuki Hatano, and other lab members of the M.K. laboratory for discussion and comments on the manuscript. This work was supported by a Wellcome Trust Senior Investigator Award (WT101885MA), a Royal Society Wolfson merit award (WM130042), and a European Research Council Advanced Grant (ERC-2014-ADG No. 671083) to M.K.B.

REFERENCES

Balasubramanian MK, McCollum D, Chang L, Wong KCY, Naqvi NI, He X, Sazer S, Gould KL (1998). Isolation and characterization of new fission yeast cytokinesis mutants. Genetics 149, 1265–1275.

Bezanilla M, Forsburg SL, Pollard TD (1997). Identification of a second myosin-II in *Schizosaccharomyces pombe*: Myp2p is conditionally required for cytokinesis. Mol Biol Cell 8, 2693–2705.

Bhattacharjee R, Mangione MSC, Wos M, Chen JS, Snider CE, Roberts-Galbraith RH, McDonald NA, Presti LLo, Martin SG, Goulda KL (2020). DYRK kinase Pom1 drives F-BAR protein Cdc15 from the membrane to promote medial division. Mol Biol Cell 31, 917–929.

Chang F, Drubin D, Nurse P (1997). Cdc12P, a protein required for cytokinesis in fission yeast, is a component of the cell division ring and interacts with profilin. J Cell Biol 137, 169–182.

Chang F, Woollard A, Nurse P (1996). Isolation and characterization of fission yeast mutants defective in the assembly and placement of the contractile actin ring. J Cell Sci 109 (Pt 1), 131–142.

Chew TG, Huang J, Palani S, Sommese R, Kamnev A, Hatano T, Gu Y, Oliferenko S, Sivaramakrishnan S, Balasubramanian MK (2017). Actin turnover maintains actin filament homeostasis during cytokinetic ring contraction. J Cell Biol.

Clifford DM, Wolfe BA, Roberts-Galbraith RH, McDonald WH, Yates JR, Gould KL (2008). The Clp1/Cdc14 phosphatase contributes to the robustness of cytokinesis by association with anillin-related Mid1. J Cell Biol 181, 79–88.

Eng K, Naqvi NI, Wong KCY, Balasubramanian MK (1998). Rng2p, a protein required for cytokinesis in fission yeast, is a component of the actomyosin ring and the spindle pole body. Curr Biol 8, 611–621.

Fankhauser C, Reymond A, Cerutti L, Utzig S, Hofmann K, Simanis V (1995). The *S. pombe* cdc15 gene is a key element in the reorganization of F-actin at mitosis. Cell 82, 435–444.

Fujiwara K, Pollard TD (1976). Fluorescent antibody localization of myosin in the cytoplasm, cleavage furrow, and mitotic spindle of human cells. J Cell Biol 71, 848–875.

Guha M, Zhou M, Wang YL (2005). Cortical actin turnover during cytokinesis requires myosin II. Curr Biol 15, 732–736.

Kitayama C, Sugimoto A, Yamamoto M (1997). Type II myosin heavy chain encoded by the myo2 gene composes the contractile ring during cytokinesis in *Schizosaccharomyces pombe*. 137, 1309–1319.

Laplante C, Huang F, Tebbs IR, Bewersdorf J, Pollard TD (2016). Molecular organization of cytokinesis nodes and contractile rings by super-resolution fluorescence microscopy of live fission yeast. Proc Natl Acad Sci 113, E5876–E5885.

Laporte D, Coffman VC, Lee IJ, Wu JQ (2011). Assembly and architecture of precursor nodes during fission yeast cytokinesis. J Cell Biol 192, 1005–1021.

Matsuyama A, *et al*. (2006). ORFeome cloning and global analysis of protein localization in the fission yeast *Schizosaccharomyces pombe*. Nat Biotechnol 24, 841–847.

May KM, Watts FZ, Jones N, Hyams JS (1997). Type II myosin involved in cytokinesis in the fission yeast, *Schizosaccharomyces pombe*. Cell Motil Cytoskeleton 38, 385–396.

Mcdonald NA, Vander Kooi CW, Ohi MD, Gould KL (2015). Oligomerization but not membrane bending underlies the function of certain F-BAR proteins in cell motility and cytokinesis. Dev Cell.

Mcdonald NA, Lind AL, Smith SE, Li R, Gould KL (2017). Nanoscale architecture of the *Schizosaccharomyces pombe* contractile ring. Elife 6, 1–23.

Mishra M, Karagiannis J, Trautmann S, Wang H, McCollum D, Balasubramanian MK (2004). The Clp1p/Flp1p phosphatase ensures completion of cytokinesis in response to minor perturbation of the cell division machinery in *Schizosaccharomyces pombe*. J Cell Sci 117, 3897–3910.

Moreno S, Klar A, Nurse P (1991). [56]Molecular genetic analysis of fission yeast Schizosaccharomyces pombe. Methods Enzymol 194, 795–823.

Motegi F, Nakano K, Kitayama C, Yamamoto M, Mabuchi I (1997). Identification of Myo3, a second type-II myosin heavy chain in the fission yeast *Schizosaccharomyces pombe*. FEBS Lett 420, 161–166.

Nurse P, Thuriaux P, Nasmyth K (1976). Genetic control of the cell division cycle in the fission yeast *Schizosaccharomyces pombe*. Mol Gen Genet 146, 167–178.

Okada H, Wloka C, Wu JQ, Bi E (2019). Distinct roles of myosin-ii isoforms in cytokinesis under normal and stressed conditions. IScience 14, 69–87.

Pelham RJ, Chang F (2002). Actin dynamics in the contractile ring during cytokinesis in fission yeast. Nature 419, 82–86.

Pollard TD, O'Shaughnessy B (2019). Molecular mechanism of cytokinesis. Annu Rev Biochem 88, 661–689.

Ren L, Willet AIH, Roberts-Galbraith RH, McDonald NA, Feoktistova A, Chen J-S, Huang H, Guillen R, Boone C, Sidhu L, *et al*. (2015). The Cdc15 and Imp2 SH3 domains cooperatively scaffold a network of proteins that redundantly ensure efficient cell division in fission yeast. Mol Biol Cell 26, 256–269.

Roberts-Galbraith RH, Ohi MD, Ballif BA, Chen J-SS, McDonald WH, Gygi SP, Iii JR, Kathleen L, McLeod I, McDonald WH, *et al*. (2010). Dephosphorylation of F-BAR protein Cdc15 modulates its conformation and stimulates its scaffolding activity at the cell division site. Mol Cell 39, 86–99.

Roberts-Galbraith RH, Chen JS, Wang J, Gould KL (2009). The SH3 domains of two PCH family members cooperate in assembly of the schizosaccharomyces pombe contractile ring. J Cell Biol 184, 113–127.

Schmidt S, Sohrmann M, Hofmann K, Woollard A, Simanis V (1997). The Spg1p GTPase is an essential, dosage-dependent inducer of septum formation in Schizosaccharomyces pombe. Genes Dev 11, 1519–1534.

Schroeder TE (1973). Actin in dividing cells: contractile ring filaments bind heavy meromyosin. Proc Natl Acad Sci USA 70, 1688–1692.

Simanis V (2015). Pombe's thirteen—control of fission yeast cell division by the septation initiation network. J Cell Sci 128, 1465–1474.

Sohrmann M, Fankhauser C, Brodbeck C, Simanis V (1996). The dmf1/mid1 gene is essential for correct positioning of the division septum in fission yeast. Genes Dev 10, 2707–2719.

Swaffer MP, Jones AW, Flynn HR, Snijders AP, Nurse P (2018). Quantitative phosphoproteomics reveals the signaling dynamics of cell-cycle kinases in the fission yeast *Schizosaccharomyces pom*be. Cell Rep 24, 503–514.

Ullal P, McDonald NA, Chen JS, Presti Lo L, Roberts-Galbraith RH, Gould KL, Martin SG (2016). The DYRK-family kinase Pom1 phosphorylates the F-BAR protein Cdc15 to prevent division at cell poles. J Cell Biol 137, 341–353.

Wachtler V, Huang Y, Karagiannis J, Balasubramanian MK (2006). cell cycle-dependent roles for the fch-domain protein cdc15p in formation of the actomyosin ring in *Schizosaccharomyces pombe*. Mol Biol Cell 16.

Win TZ, Gachet Y, Mulvihill DP, May KM, Hyams JS (2001). Two type V myosins with non-overlapping functions in the fission yeast *Schizosaccharomyces pombe*: Myo52 is concerned with growth polarity and cytokinesis, Myo51 is a component of the cytokinetic actin ring. J Cell Sci 114, 69–79.

Wollrab V, Thiagarajan R, Wald A, Kruse K, Riveline D (2016). Still and rotating myosin clusters determine cytokinetic ring constriction. Nat Commun 7.

Wong KCY, D'Souza VM, Naqvi NI, Motegi F, Mabuchi I, Balasubramanian MK (2002). Importance of a myosin II-containing progenitor for actomyosin ring assembly in fission yeast. Curr Biol 12, 724–729.

Wood V, Harris M, McDowall M, Rutherford K, Vaughan B, Staines D, Aslett M, Lock A, Bähler J, Kersey P, *et al*. (2012). PomBase: A comprehensive online resource for fission yeast. Nucleic Acids Res 40, 695–699.

Wu J-Q, Pollard TD (2005). Counting cytokinesis proteins globally and locally in fission yeast. Science (80-) 310, 310–314.

Wu JQ, Bähler J, Pringle JR (2001). Roles of a fimbrin and an alpha-actinin-like protein in fission yeast cell polarization and cytokinesis. Mol Biol Cell 12, 1061–1077.

Wu JQ, Kuhn JR, Kovar DR, Pollard TD (2003). Spatial and temporal pathway for assembly and constriction of the contractile ring in fission yeast cytokinesis. Dev Cell 5, 723–734.

Yonetani A, Lustig RJ, Moseley JB, Takeda T, Goode BL, Chang F (2008). Regulation and Targeting of the Fission Yeast Formin cdc12p in Cytokinesis. Mol Biol Cell 19, 2208–2219.

Yumura S (2001). Myosin II dynamics and cortical flow during contractile ring formation in *Dictyostelium* cells. J Cell Biol 154, 137–145.

Zhang D, Vjestica A, Oliferenko S (2010). The cortical ER network limits the permissive zone for actomyosin ring assembly. Curr Biol 20, 1029–1034.